International Journal of Multiphase Flow 36 (2010) 273–283

Contents lists available at ScienceDirect

International Journal of Multiphase Flow

journal homepage: www.elsevier.com/locate/ijmulflow

Simulating compressible gas bubbles with a smooth volume tracking 1-Fluid method

G. Pianet [a,*], S. Vincent [a,*], J. Leboi [a], J.P. Caltagirone [a], M. Anderhuber [b]

[a] Université de Bordeaux, Laboratoire Transferts Écoulements Fluides Énergétique/site ENSCBP, UMR CNRS 8508, 16 Av. Pey–Berland, 33607 PESSAC, France
[b] ArcelorMittal Maizières, R&D Industrial Operations – BP 30320, F-57283 Maizières-lès-Metz Cedex, France

ARTICLE INFO

Article history:
Received 26 March 2009
Received in revised form 17 November 2009
Accepted 1 December 2009
Available online 12 January 2010

Keywords:
1-Fluid model
Penalty method
Volume tracking
Rising bubble
VOF–PLIC
Compressible gas injection

ABSTRACT

The physical relevance of an improved front-capturing 1-Fluid method is investigated considering the behavior of either incompressible or compressible gas bubbles driven by buoyancy in a two-dimensional framework. Through the coupling of a VOF–PLIC technique and a smoothing function of adjustable thickness, the Smooth Volume of Fluid technique SVOF is intended to capture accurately strong interface distorsion with large density and viscosity contrasts between phases, combined with the front-capturing automatic treatment of interface rupture or reconnection. The fundamental idea lies in using the regular VOF–PLIC technique, while applying a smoothing procedure affecting both physical characteristics averaging and surface tension modeling. A thorough assessment procedure is achieved comparing the present method, front-tracking simulations and experiments from Bhaga and Weber that characterize the shape and velocity of single gas bubbles rising into liquid columns. A series of 200 SVOF simulations was necessary to provide a unique set of smoothing and averaging parameters available for any kind of bubble that is stable in an axisymmetric framework. The front-capturing strategy greatly eases the extension to gas injection applications as there is no micro-management required during interface coalescence or break-up, and no volume correction either. Finally the robustness of the 1-Fluid SVOF method is demonstrated in two-dimensions, in the case of compressible or incompressible gas injection into cold metal alloys where the density ratio between phases is greater than 3500.

1. Introduction

Multiphase systems modeling is concerned with a very wide range of industrial and environmental applications. The present work was motivated by the need for predicting the efficiency of gas-jet penetration and break-up in molten metals. Such systems are extremely aggressive and opaque to most experimental investigation techniques, so that simulation methods are probably the only relevant way to gain insight into physical mechanisms. What make things difficult is that molten metals are extremely dense and their viscosity very low, so that depending on the bubble size and velocity, simulation methods should be effective for a very large number of possible flow regimes. Numerical challenges consist in preserving sharp interfaces, ensuring mass and momentum balance with a realistic approach for coalescence or rupture phenomena.

Over the past 10 years a wide set of direct numerical methods has been specifically designed to address those complex issues. Excellent accuracy is generally achieved with surface tracking methods, notably the front-tracking method (Unverdi and Tryggvason, 1992; Hua and Lou, 2007), the Level-Set methods (Osher and Fedkiw, 2003; Tanguy and Berlemont, 2005) or the Adaptative Lagrange Euler method (Yue et al., 2007). The marker-based surface tracking approach is a relevant strategy when simulating isolated droplets or bubbles, with a restriction to flows with few vorticity sources therefore with few occurrences of interface breakup or merging. Those issues can be addressed either manually or using complex sub-grid models. Moreover Lagrangian techniques require dynamic re-meshing of the interfacial grid to prevent surface nodes or markers from aggregating or rarefying. Level-Set methods are arguably best-suited to handling breakup or merging but mass conservation and accuracy are degraded when flows generate large interface distortion. It has also been reported by Hua and Lou (2007) that volume control and correction is necessary when using front-tracking approaches. Alternatively, Lagrangian tracking can also be performed on particles dispersed within a volume cell, this is the famous Particles in Cells method (PIC, see Harlow and Welch, 1965) that overcome most of the preceding difficulties, at the expense of very large computing resources.

When preserving mass and assuming large interface discontinuities becomes a critical issue, one can consider front-capturing strategies in which interface position is described implicitly via an Eulerian framework. This is the general Volume of Fluid (VOF)

* Corresponding authors. Tel.: +33 2 32 53 63 51; fax: +33 2 32 53 64 68 (G. Pianet), tel.: +33 5 40 00 27 07; fax: +33 5 40 00 66 68 (S. Vincent).
E-mail addresses: gregoire.pianet@cnpp.com (G. Pianet), vincent@enscbp.fr (S. Vincent).

0301-9322/$ - see front matter © 2009 Elsevier Ltd. All rights reserved.
doi:10.1016/j.ijmultiphaseflow.2009.12.002

approach where a local phase volume fraction is introduced to capture interface. The reader is referred to the detailed report of recent VOF approaches (see Gopala and van Wachem, 2008; Bonometti and Magnaudet, 2007). The accuracy of VOF predictions is actually lower than front-tracking accuracy when capillary effects are under consideration, but VOF ability to deal with interface rupture or coalescence and to preserve mass under large fluid distortion makes it a good candidate for capturing grid-scale features of complex two-phase flows. Drawbacks are related to three-dimensional implementation which is quite difficult, and related to numerical artifacts occurring when interface thickness is reduced below the grid-scale. In that particular case, excessive breakage is a numerical artifact. Alternatively, interface tracking and VOF methods could be used together and a fair amount of hybrid techniques have been documented in literature, one can cite for example front-tracking and VOF (Tryggvason et al., 2001), front-tracking and Level-Set (Shin and Juric, 2002) or Level-Set and VOF (Bonometti and Magnaudet, 2007). These methods were accurately assessed but drawbacks inherent to front-tracking or Level-Set are still issues to be addressed. Accurate techniques were borrowed from the phase-field approach, as shown by Jamet et al. (2001) or in the work of Inamuro et al. (2004) from a Lattice-Boltzmann formulation, but diffuse interface methods are generally too smooth to consider disperse flow undergoing large velocity gradients.

As aforementioned, our work was motivated by the prediction of either compressible or incompressible gas injection in liquid systems with unusually high viscosity and density gradients, and large fluid distortion. VOF–PLIC approaches are specially indicated in this case as they are formally volume-preserving schemes, and geometrically diffused only over a single cell length scale. Our view is that any smoothing or regularizing operator on the VOF function will alter those fundamental properties. It has been found instead that using indirectly a smooth interface for calculating fluid characteristics averaging and surface tension terms improves interface transport by significantly reducing spurious currents and artificial break-up. Concerning the underlying model framework, we have used the 1-Fluid model developed by our team (see Vincent and Caltagirone, 1999, 2000; Caltagirone and Vincent, 2001) and inspired by volume penalty methods in fictitious domains (Khadra et al., 2000) and interface reconstruction (Scardovelli and Zaleski, 1999).

In the next section, the 1-Fluid model is briefly presented, then in a more significant part it is described how the smoothing operator is used with different interpolation techniques. Section 2 includes a brief description of our strategy to cope with gas phase compressibility. In the last subsection SVOF method is thoroughly verified and compared to existing interface tracking methods. In Section 3, a rigorous assessment procedure is summarized, that firstly discriminates between the numerical parameters and interpolation schemes, and secondly demonstrates the convergence in space of the best parameter set. Predictions from those optimized settings are then compared to bubble shapes and velocity as described in the experimental work of Bhaga and Weber (1981). Section 4 is concerned with the global robustness of this approach, experienced with an example application of two-dimensional gas injection in liquid metal. Concluding remarks are addressed in the last section.

2. Numerical method

2.1. Principles of the 1-Fluid model

The numerical modeling of two-phase flows involving separated phases can be achieved with a 1-Fluid (1F) model (see Kataoka, 1986; Scardovelli and Zaleski, 1999). The 1F approach consists in integrating the interfacial jump conditions, valid at the interface (Delhaye, 1974), into the Navier–Stokes equations, valid in each phase. The integration is done by means of a convolution and a spatial filtering of the momentum equations in each phase. The resulting 1F model is similar to the single phase Navier–Stokes equations, in which extra–terms have been added so that local modifications of equations are included through local viscosities $\mu(x,y,z,t)$, densities $\rho(x,y,z,t)$ and surface tension forces. In that sense, the 1F method has similarities with the fictitious domain approach of Glowinski et al. (2001) and with the Immersed Boundary Method of Peskin (1977).

Great advantages are found by using a single set of equations in the whole calculation domain obtained by introducing a phase function $C(x,y,z,t)$ as a local description of the fluid state, used in order to follow the multiphase topology of the flow by solving an advection equation. In this work the dispersed gas phase is characterized by $C=1$ and the continuous phase by $C=0$. Interface position is defined by $C=0.5$. Therefore it is possible to express the global properties of the mixture as functions of C, namely the density $\rho=f(C)$ and dynamic viscosity $\mu=g(C)$. Very few reference works exist that compare and demonstrate the right form of $f(C)$ and $g(C)$. Such a form is obtained for example using linear interpolation of characteristics: $\mu=\mu_l(1-C)+\mu_g C$ and $\rho=\rho_l(1-C)+\rho_g C$, where the subscripts l and g represent, respectively, the liquid or gas phases. Several numerical methods for evaluating $\rho=f(C)$ and $\mu=g(C)$ will be presented and discussed later. This aspect is of major importance for the numerical simulation of multiphase flows.

The final set of equations used to build the 1-Fluid model comprises the Navier–Stokes Eqs. (1), an advection equation on the phase function (2), and the incompressibility constraint (3):

$$\rho\left(\frac{\partial \mathbf{u}}{\partial t}+(\mathbf{u}\cdot\nabla)\mathbf{u}\right)=\rho\mathbf{g}-\nabla p+\nabla\cdot(\mu(\nabla\mathbf{u}+\nabla^t\mathbf{u}))+\mathbf{F}_{st}, \tag{1}$$

$$\frac{\partial C}{\partial t}+\mathbf{u}\cdot\nabla C=0, \tag{2}$$

$$\nabla\cdot\mathbf{u}=0, \tag{3}$$

where $\mathbf{u}$ is the local velocity field, t the time, p the pressure, $\mathbf{g}$ the gravity field and $\mathbf{F}_{st}$ is the surface tension force. According to the CSF model of Brackbill et al. (1992), forces due to capillarity can be expressed in the following form:

$$\mathbf{F}_{st}=\sigma\kappa\mathbf{n}_i\delta_i, \tag{4}$$

where σ is the surface tension coefficient, κ the local curvature of the interface, $\mathbf{n}_i$ the normal to the interface and δ_i is the Dirac function indicating interface. In this paper, the equation set (1)–(3) is then referred to as the incompressible 1-Fluid model.

2.2. Penalty-based compressibility approach

Based on the incompressible model (1)–(3), a multiphase compressible model for isothermal flows can be built (see Caruyer et al., 2009), which takes into account the local volume dilatation and compression effects under flow constraints. A specific divergence term is added into the momentum equations and a modified mass conservation equation is introduced in this case. This 1F compressible model is correct under a low Mach number assumption:

$$\rho\left(\frac{\partial \mathbf{u}}{\partial t}+(\mathbf{u}\cdot\nabla)\mathbf{u}\right)=\rho\mathbf{g}-\nabla\left(p-\frac{\tau}{\chi_T}\nabla\mathbf{u}\right)+\nabla\cdot(\mu(\nabla\mathbf{u}+\nabla^t\mathbf{u}))+\mathbf{F}_{st}, \tag{5}$$

$$\frac{\partial C}{\partial t}+\mathbf{u}\cdot\nabla C=0, \tag{6}$$

$$\frac{\partial p}{\partial t}+\frac{1}{\chi_T}\nabla\cdot\mathbf{u}=0, \tag{7}$$

where χ_T is the isothermal compressibility coefficient of the local phase. χ_T can be either imposed or calculated from an equation of state. Parameter τ is a characteristic compression time scale. In the context of this paper, all macroscopic scales are considered to be fully captured following direct numerical simulation principles. The smallest spatial scale is related to local pressure waves so that τ is assumed to be of the order of the simulation time scale Δt. Ratio τ/χ_T in Eq. (5) can be defined as a coefficient of resistance to compression, similar to the compression viscosity coefficient λ.

2.3. General computational methodology

Finite volume discretizations on fixed Cartesian grids are applied to approximate the conservation equations. Concerning the resolution of both incompressible (1)–(3) and compressible (5)–(7) Navier–Stokes equations, and in either case, for solving the velocity–pressure coupling, the augmented Lagrangian method of Fortin and Glowinski (1982) was used. In order to satisfy the fluid incompressibility in the incompressible version of the 1F model, the augmented Lagrangian method has been previously adapted to multiphase flows (Vincent et al., 2004, 2007). All of the terms appearing in Eq. (1) are spatially discretized via a second order accurate centered scheme. A second order accurate Gear scheme is implemented for the discretization of the time dependent term. Implicit discretization of the momentum equations necessarily requires the linearization of the convective term $(\mathbf{u}\cdot\nabla)\mathbf{u}$ that takes the form $(\mathbf{u}^n\cdot\nabla)\mathbf{u}^{n+1}$. The resulting algebraic system is inverted by the direct solver called MUMPS Amestoy et al. (2000).

The advection Eq. (2) is hyperbolic and is applied to a discontinuous Volume of Fluid function C. One numerical approach for solving this equation is the implementation of monotone Total Variation Diminishing TVD (see Vincent and Caltagirone, 1999) or Weighed Essentially Non-Oscillating WENO schemes of Jiang and Shu (1996). Such schemes are able to handle correctly the high gradients located on liquid–gas interfaces. They produce numerical diffusion that is maintained over a few grid cells across the interface. However, as soon as strong vorticity sources appear in the flow motion, this numerical diffusion is increased and the interface spreads over too many grid cells. This major drawback is avoided using a different numerical technique for approximating Eq. (2): the Piecewise Linear Interface Construction (PLIC) VOF method of Youngs et al. (1982). This approach relies on a geometrical approximation of the interface in each grid cell by linear or planar elements, which are advected in a Lagrangian way following the local normal direction to the interface.

All the previous numerical methods have been extensively presented and validated in previous works by the authors (Vincent and Caltagirone, 1999, 2000; Vincent et al., 2004, 2007, 2008).

2.4. Discrete surface tension models

The principle drawback of recent VOF methods is associated to the generation of small artificial blobs occurring when the characteristic lengthscale of interfaces is comparable to the local grid size. Moreover, the discretization of the surface tension force requires the approximation of second order partial derivatives of the VOF function, whose gradients are conceptually restricted to one cell. As a consequence, the compact support of the discrete surface tension force, which relies on centered schemes following the work of Brackbill et al. (1992), is incomplete, since the VOF function only varies on a single cell length-scale. As aforementioned in the introduction section, our main idea lies in building an auxiliary Smooth VOF (SVOF) function called C^S, which will be obtained thanks to C, but will not explicitly replace this sharp VOF function, in order to keep the right mass conservation features brought by the PLIC numerical algorithm of Youngs et al. (1982). However the SVOF function should match the interface position, so that condition $C(M)=0.5$ is met in the same cells as those in which $C^S(M)=0.5$ at a given position M. In this way, the averaging procedures that are required to build ρ and μ, will be based on C^S and will characterize the same fluid sub-domains as C. The SVOF averaging and surface tension forces will be detailed in the next sections.

The parameterization of the SVOF equation has been carried out by analogy with the unsteady diffusion equation for thermal transfers:

$$\frac{\partial T}{\partial t}-\nabla\cdot a\nabla T=0, \tag{8}$$

considering $a>0$ as the thermal diffusivity coefficient. It is known that the diffusion length δ is equal to $\sqrt{a\tau_d}$, where τ_d is the characteristic time scale of diffusion. Assuming $a=1,\tau_d$, and δ^2 are of the same order. By discretizing T in time, with n the time index corresponding to time $n\Delta t$ and Δt the numerical time step, we obtain:

$$-\nabla\cdot\tau_d\nabla T^{n+1}+T^{n+1}=T^n. \tag{9}$$

If Eq. (9) is solved N times, with $1\leqslant n\leqslant N-1,\tau_d=N\Delta t$ and the initial temperature field $T^0=C$, it is ensured that T diffuses on a length equal to δ and that $T=T^0$ far from the diffusion zone, i.e. the zone where temperature gradients are zero.

By analogy with the previous thermal developments, the SVOF method consists in building a smooth VOF function C^S by iteratively solving a Helmholtz equation with the initial condition $C^{S,0}$ equal to the sharp VOF function C:

$$-\nabla\cdot D\nabla C^{S,n+1}+C^{S,n+1}=C^{S,n}, \tag{10}$$

where the diffusion coefficient D is equal to $L_i\Delta h^2$. This parameter is fixed in order to ensure that the VOF function C^S spreads over a distance L_i on each side of the interface $C=0.5$. The coefficient Δh is equal to the local characteristic size of the grid cell. From a numerical point of view, Eq. (10) is implicitly discretized in space using finite volume conventions with a centered scheme, in such a way as to be consistent with the Navier–Stokes equation approximation, and the resulting linear system is solved with the direct MUMPS solver of Amestoy et al. (2000). Finally, the numerical algorithm for obtaining C^S is:

$$F^1=C, \tag{11}$$

$$\text{For } k=1\ldots N-1,\ \text{solve} \tag{12}$$

$$-\nabla\cdot\tau_d^*\nabla C^{S,k+1}+C^{S,k+1}=F^k, \tag{13}$$

$$F^{k+1}=C^{S,k+1}, \tag{14}$$

where τ_d^* is defined as $L_i\Delta h^2/N$. After solving algorithm (12)–(14), the condition $C^S=C^{S,k+1}=C^{S,N}$ is verified. An example of SVOF function obtained on a grid sample is presented in Fig. 1. This figure compares functions C and C^S. There it is demonstrated that isoline $C^S=0.5$ is smoother than $C=0.5$ and that the diffusion zone associated to C^S following the normal to the interface is of regular thickness.

2.5. Comparison of SVOF method to existing interface tracking methods

The ability of the SVOF method to handle accurately bubble or droplet dynamics compared to existing interface tracking techniques is investigated. The test case 1 from the benchmark proposed by Hysing et al. (1999) is used to evaluate the performances of the SVOF approach by comparison to numerical results from the front-tracking method (see Shin and Juric, 2002) and the Level-Set method (see Osher and Fedkiw, 2003; Trontin et al., 2008). The initial configuration of the problem is presented in Fig. 2.

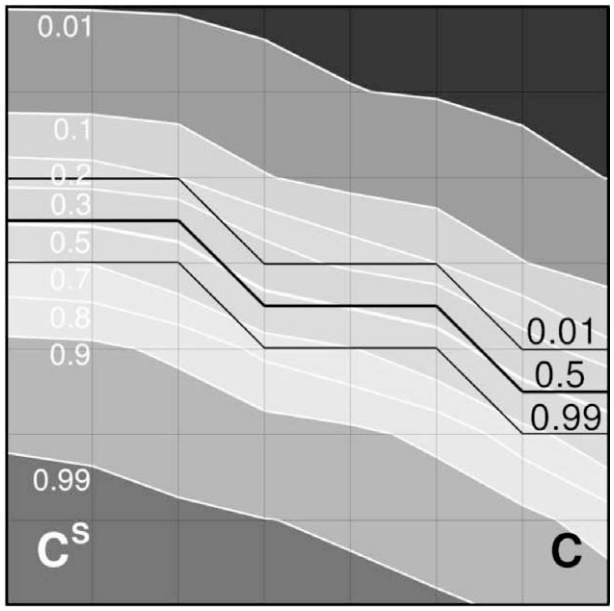

Fig. 1. Comparison of VOF function C, and Smoothed VOF function C_S.

The fluid characteristics are the following: the density and the dynamic viscosity in fluid 1 are 1000 kg m^{-3} and 10 Pa s whereas these parameters are equal, respectively, to 100 kg m^{-3} and 1 Pa s in fluid 2. The gravity magnitude is 9.81 m s^{-2} according to the vertical direction, and the surface tension coefficient is 24.5 N m^{-1}.

Some qualitative comparisons of the interfacial position provided by SVOF, Level-Set and front-tracking methods at a time $t = 3$ s are proposed in Fig. 3. All numerical solutions are in good agreement with the results from Hysing et al. (1999) obtained using a Level-Set approach: the bubble shape is included in the range $0.15 < x < 0.85$ and $0.9 < z < 1.3$. However, small differences are observed: the front-tracking solution is smoother than the Level-Set results and the Lagrangian interface tracking approach provides a slightly larger growing bubble velocity on the finer mesh than the SVOF and Level-Set techniques. As no analytical solution exist for the bubble dynamics, it is difficult to choose a reference solution, even though the front-tracking solution is known to be very accurate and efficient to account for capillary effects in bubbly flows (Esmaeeli and Tryggvason, 1998).

Concerning the SVOF method, a good space and time convergence is observed in Fig. 4. The $C = 0.5$ contour level is plotted at time $t = 3$ s. In order to estimate the numerical performances of the interface tracking methods, the error on volume conservation $E_{vol} = \int_\Omega C(t = 3\text{ s})dV - \int_\Omega C(t = 0\text{ s})dV$ as well as the computational time obtained on an Intel Centrino processor are considered.

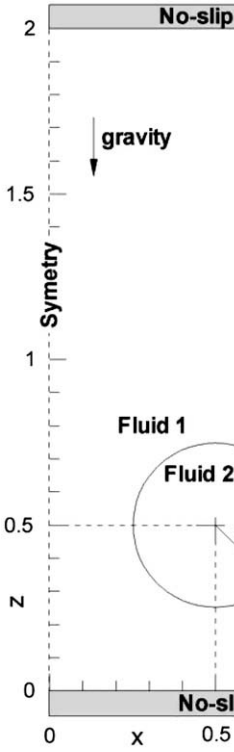

Fig. 2. Definition sketch of the benchmark proposed by Hysing et al. (1999).

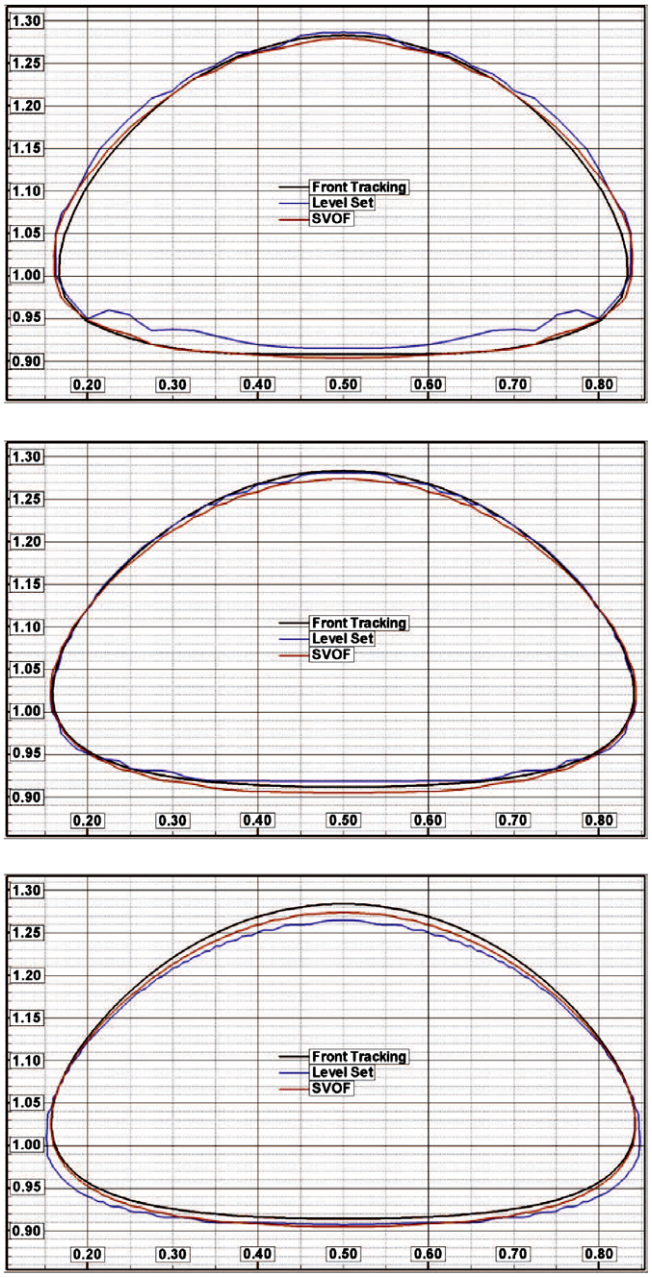

Fig. 3. Comparison of the front-tracking, Level-Set and SVOF methods on three different grids (40×80 in the top image, 80×160 in the centered image and 160×320 in the bottom image).

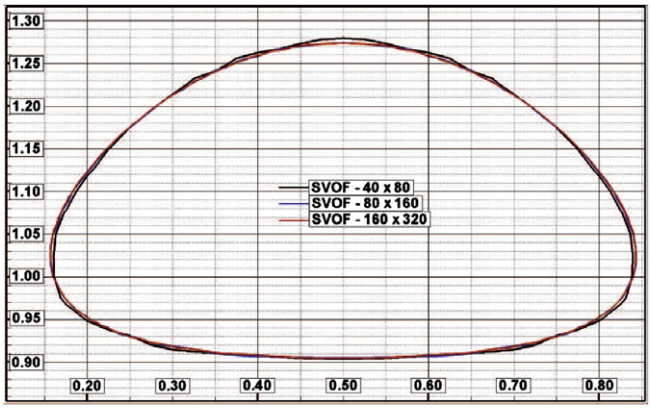

Fig. 4. Convergence of the interface provided by the SVOF method.

Notation Ω refers to the computational domain. These values are reported in Table 1.

Considering mass conservation which is evaluated by E_{vol}, it is observed that the SVOF method achieves the best results, this is made clear as the grid level is refined. The front-tracking approach comes in second place as the Level-Set achieves the worst results. These observations are in agreement with the known numerical behaviors of the front-tracking and Level-Set methods which do not intrinsically maintain the mass conservation. It can be stressed that the gap between the front-tracking and the SVOF methods is small concerning volume error. But this is offset by the higher consumption in time of the SVOF method, an overcost due to the solving of an implicit Helmholtz equation to build the smooth function C^S. The computational time is almost comparable between the front-tracking and the Level-Set techniques. On the coarser grid, the overcost of the SVOF is 31% compared to the front-tracking method while this increase in time is reduced to 19% on the finest mesh. The larger the computational grid, the smaller the gap between the SVOF and the front-tracking computational time will be, as the time required to solve Navier–Stokes equations overcomes other computational steps.

To finish with, a convergence order of the interface tracking methods can be achieved by considering the decreasing of E_{vol} according to the number of computational nodes. The values obtained with 80×160 and 160×320 grids are considered. It is observed that E_{vol} is divided by 3.6 with the SVOF method when the space step Δx is divided by 2, which corresponds to a 1.85 convergence order in space. For the Level-Set approach, E_{vol} is reduced by a factor 2.08 when Δx is divided by 2, which corresponds to a 1.06 convergence order in space. For the front-tracking method, E_{vol} is divided by 3.8 in the same conditions and a 1.93 space convergence order is obtained.

3. SVOF assessment

3.1. Setup of numerical experiments

Buoyancy driven phenomena in gas–liquid flows are long-standing research issues, this is why a large body of recent literature is still interested in characterizing the transient aspect of a single gas bubble rising in viscous liquids. In this section, numerical predictions are compared to the experimental contribution from Bhaga and Weber (1981). The main result consists in a complete regime map reported in Fig. 5. The shape of one isolated bubble depends upon Reynolds number $Re = \rho_f d U_t / \mu_f$ and Bond number $Bo = \rho_f g U_t / \sigma$, where ρ_f and μ_f are the fluid density and viscosity, $d = (6V_b/\pi)^{1/3}$ the effective bubble diameter based on bubble volume V_b, U_t the terminal bubble velocity and σ the surface tension between both phases. Recently, numerical prediction from Hua and Lou (2007) confirmed that when physical parameters satisfy $(\mathrm{Re} < 200, \mathrm{Bo} < 200)$ (see dashed box in Fig. 5), both bubble shape and velocity field obey axial symmetry. Therefore validations in two-dimensions are feasible in this particular range and axisymmetry hypothesis is assumed in the present work if not mentioned otherwise.

Domain size and aspect ratio relative to bubble size are fixed by default in a way similar to the procedure from Hua and Lou (2007). At time $t = 0$, the bubble is a sphere of diameter d which is placed $2d$ away from the bottom, $10d$ away from the top and $4d$ away from the side, as reported in Fig. 6. Eight different test-cases were defined in order to match data from Bhaga and Weber (1981) (see 'A' series plotted in Fig. 5). Density ratio $\rho^* = \rho_f/\rho_g$ is fixed at 773, dynamic viscosity ratio $\mu^* = \mu_f/\mu_g$ is set between 1300 and 489400, and surface tension σ is ranging from 6×10^{-3} to 4.53×10^{-1} N/m.

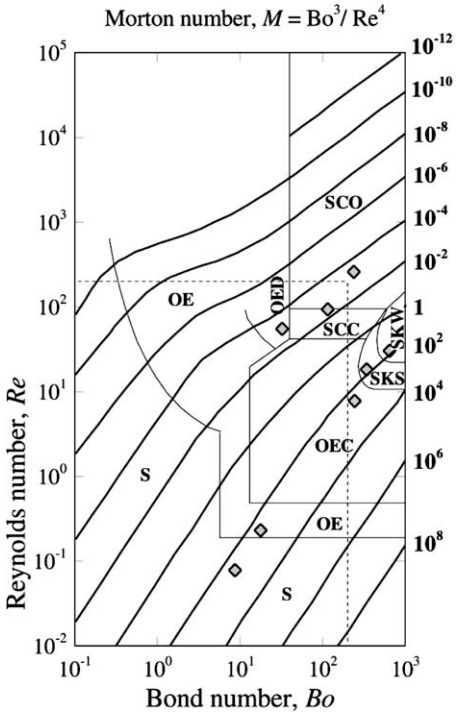

Fig. 5. Regime Map of rising bubbles as reported by Bhaga and Weber (1981), from lowest to highest Re number: [S] Spherical (A1), [OE] Oblate Ellipsoid (A2), [OEC] Oblate Ellipsoidal Cap (A4), [SKS] Skirted Steady (A7), [SKW] Skirted Wavy (A8), [OED] Oblate Ellipsoidal (A3), [SCC] Spherical Cap Closed wake (A5), [SCO] Spherical Cap Open wake (A6).

Table 1
Comparison of errors on volume and computational times for SVOF, Level-Set and front-tracking methods on three different grids.

Grid	E_{vol} SVOF	Time (s) SVOF	E_{vol} Level-Set	Time (s) Level-Set	E_{vol} front-tracking	Time (s) front-tracking
40×80	1.51×10^{-3}	118	3.26×10^{-2}	95	1.18×10^{-3}	90
80×160	3.32×10^{-4}	898	1.36×10^{-2}	761	4.56×10^{-4}	750
160×320	9.21×10^{-5}	4314	6.54×10^{-3}	3852	1.20×10^{-4}	3620

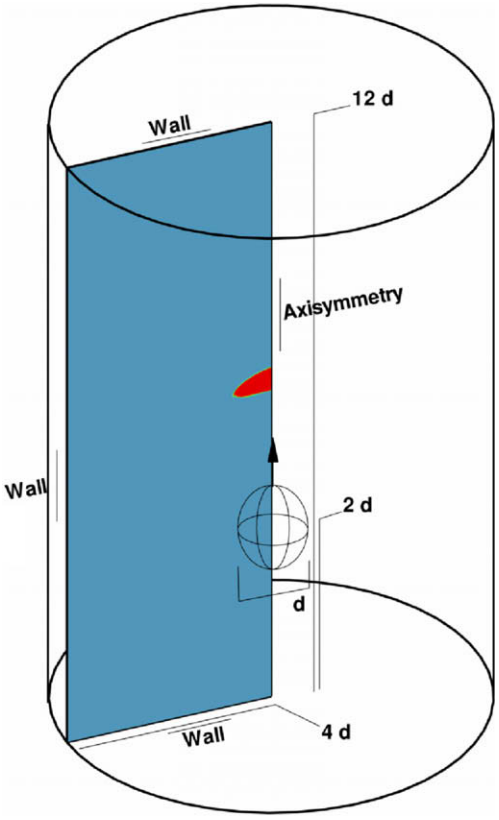

Fig. 6. Conditions of numerical experimentation.

3.2. Impact of physical characteristics averaging methods on bubble dynamics

This section is concerned with the choice of interpolation functions $f(C)$ and $g(C)$ for estimating, respectively, density ρ and viscosity μ across the interface. The way of estimating average density and viscosity at the interface neighborhood is somewhat empirical and needs rigorous testing, and particularly as characteristic gradients between gas and liquid are very high. Practically, the interpolation scheme does rule the respective weight of gas and liquid into interfacial cells. As aforementioned, very few works have been found in literature in which averaging techniques are described and thoroughly assessed, even though they are used widely. One can mention three common schemes for evaluating f(C):

(i) *discontinuous averaging*:

$$f(C) = f_g \text{ where } C > 1/2,\ f(C) = f_l \text{ elsewhere},$$

(ii) *arithmetic averaging*:

$$f(C) = f_l \cdot (1 - C) + f_g \cdot C,$$

(iii) *harmonic averaging*:

$$f(C) = f_l \cdot f_g / (f_l \cdot (1 - C) + f_g \cdot C).$$

The logic about considering harmonic averaging as an alternative to discontinuous or arithmetic averaging have been discussed in a former work by Ritz and Caltagirone (1999). Using different schemes for density and viscosity yield many potential combinations. We have reduced the number of possibilities to a set of four methods that are commonly used in multiphase flow solvers. These are, respectively, $M1$: discontinuous for both density and viscosity, $M2$: arithmetic averaging for both density and viscosity, $M5$: arithmetic averaging for density and harmonic averaging for viscosity, and finally $M7$: arithmetic averaging for density, arithmetic averaging when using diagonal components of the viscous stress tensor, and harmonic averaging when using extradiagonal components of the viscous stress tensor. Obviously, using harmonic averaging for $\rho = f(C)$ is physically meaningless, and the additive property of density is perfectly suited to linear interpolation. Fig. 7 summarizes the terminal bubble shape predicted with those four methods in comparison to experimental and front-tracking simulation results from literature.

Table 2 presents terminal bubble velocities with corresponding error levels in comparison to experimental velocities. The best overall results have been achieved with the linear interpolation for both density and viscosity ($M2$). This technique combined with interface smoothing for capillarity exhibits excellent agreement with both experimental and front-tracking simulation results. Arithmetic averaging on viscosity yields non physical surface tension features, made clear from cases A1 + M5, A2 + M5, and A3 + M5. One problematic artifact is highlighted along the symmetry axis when using methods M5 or M7, as the interface presents a non physical angle inducing over-estimated terminal velocities. The M1 technique is globally relevant considering general shapes and terminal velocities, but discontinuous averaging techniques clearly increase the numerical fragmentation of the interface. Special situations of spherical cap shaped bubbles are notably complicated to simulate, as the bubble vertical thickness almost vanishes during its acceleration so that a subresolved gas layer on the bubble axis makes it split into toroidal bubbles instead. A5 cases are generally stable with our method but non-negligible fragmentation into secondary macro-bubbles are eventually observed. A6 cases have been obtained from one ellipsoidal starting shape but produced very unstable results in general. Consequently, M2 models will be used in this work, as a very good physical consistency is achieved. Moreover, the combination of VOF–PLIC, M2 averaging and interface smoothing for capillarity, exhibits excellent interface cohesion as very little numerical fragmentation is observed compared to other combinations.

3.3. Convergence in space of SVOF, Test-Case A3 [Re = 79.9, Bo = 32.2]

Test-Case A3 has been chosen for testing spatial accuracy of those optimized settings and estimating *a priori* how many nodes are required to achieve good predictions. Simulations are performed with increasing accuracy in space readily defined as $d/\Delta x = 13, 25, 50, 100,$ and 200 where Δx is the unit grid size expressed in meters. For comparison, results from the front-tracking simulations of Hua and Lou (2007) are considered to be converged starting from $d/\Delta x = 25$ grid points. It is found that VOF–PLIC simulations do not converge exactly to the experimental value ($U_t = 2.9 \times 10^{-1}$ m/s) but to a value that is about 3% smaller. However, experimental error level on velocity is estimated to be 3.5% by the authors (Bhaga and Weber, 1981) so that SVOF result is within error bar. Small deviations from experimental values may be due to perturbations related to the numerical management of the symmetry axis. It can explain why the bubble thickness is somewhat overestimated, as seen in Fig. 7. We still have to check the same case in a fully three-dimensional framework to address this issue, knowing that no perturbations were noticed in two-dimensions. For demonstrating convergence in space, we use the Richardson's extrapolation technique (see Roache, 1998) in which the value of reference is calculated from the finest grid level simulation result. A very clear convergence in space of order 1.2 is shown in Fig. 8, showing that most physical features are captured efficiently by SVOF.

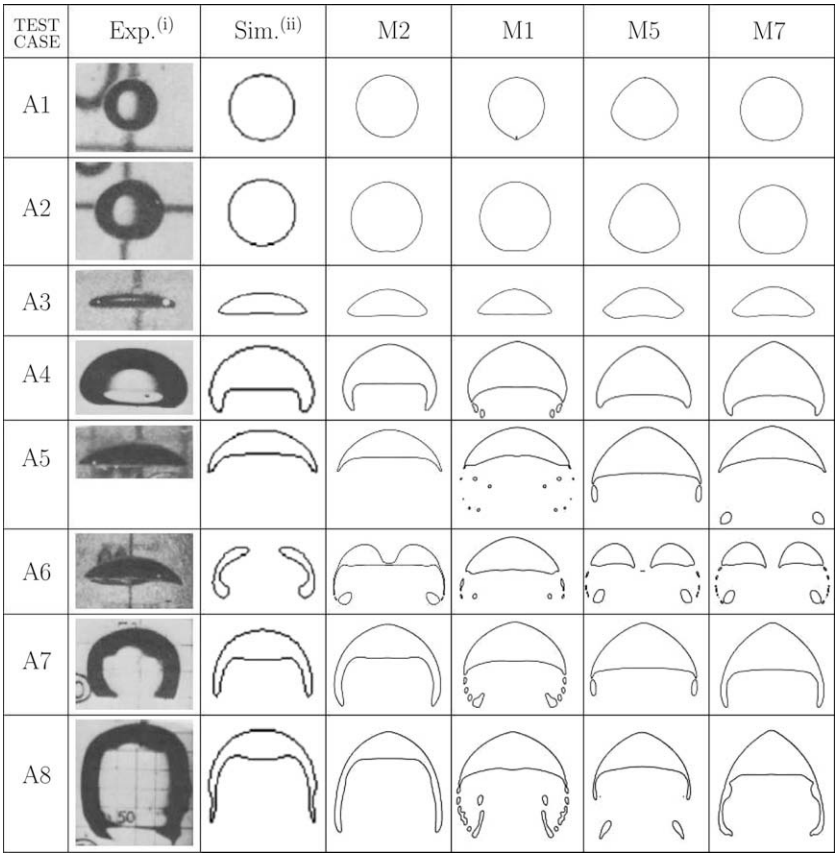

Fig. 7. Terminal bubble shape for M2, M1, M5, and M7 averaging methods. Comparison to (i) experiments of Bhaga and Weber (1981) and (ii) front-tracking simulations of Hua and Lou (2007).

Table 2
Terminal bubble rising velocity for M2, M1, M5, and M7 averaging methods. Comparison to the experimental values U_{Exp} from the work of Bhaga and Weber (1981).

Test-Case	Run#	Interpolation	U_{1F} (m s^{-1})	U_{Exp} (m s^{-1})	Error (%)	Best overall
A1	71	M1	0.0364	0.0353	3.1	
–	51	M2	0.0356	–	0.8	×
–	81	M5	0.0573	–	62.4	
–	91	M7	0.0418	–	18.4	
A2	72	M1	0.0613	0.0615	0.3	
–	52	M2	0.0599	–	2.6	×
–	82	M5	0.0890	–	44.7	
–	92	M7	0.0705	–	14.6	
A3	73	M1	0.3139	0.3066	2.3	
–	53	M2	0.3031	–	1.1	×
–	83	M5	0.3132	–	2.1	
–	93	M7	0.3103	–	1.2	
A4	74	M1	0.2465	0.2258	9.1	
–	54	M2	0.2379	–	5.3	×
–	84	M5	0.2858	–	26.5	
–	94	M7	0.2804	–	24.2	
A5	75	M1	0.3144	0.3093	1.7	
–	55	M2	0.2908	–	10.2	×
–	85	M5	0.2280	–	26.3	
–	95	M7	0.2999	–	3.0	
A7	77	M1	0.2877	0.2629	9.5	
–	57	M2	0.2774	–	5.5	×
–	87	M5	0.3236	–	23.1	
–	97	M7	0.3185	–	21.2	
A8	78	M1	0.3016	0.2699	11.7	
–	58	M2	0.2903	–	7.5	×
–	88	M5	0.3373	–	24.9	
–	98	M7	0.3411	–	26.4	

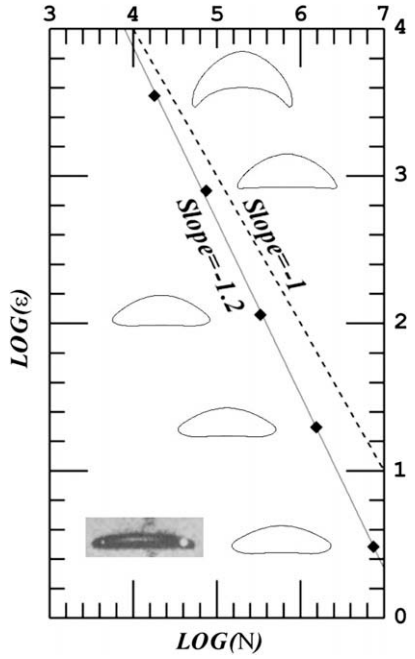

Fig. 8. Convergence in space of Test-Case A3 based on reference terminal bubble velocity value $U_t = 2.9 \times 10^{-1}$ m/s calculated with Richardson's extrapolation technique Roache (1998). Spatial discretization is defined successively as $d/\Delta x = 13, 25, 50, 100$, and 200 grid points.

4. Gas injection in liquid alloy: effect of gas compressibility

4.1. Dynamics of a single compressible gas bubble

Obviously, the first issue one should address is the effect of gas compressibility on isolated bubbles as those described in the previous section. Since very realistic predictions were obtained using the incompressible gas phase, it is therefore necessary to achieve the same level of accuracy or better within the compressible framework. After activating compressibility, one found that stabilized bubbles are very similar in shape. Results are summarized in Table 3 where the previous accuracy is shown to be globally respected and slightly improved. The initial volume is shown to be preserved, whereas bubble volume appears to be growing in both cases for increasing Reynolds numbers. With the present numerical approach, the incompressible gas phase is treated like a weakly compressible phase, so that the volume change is negligible, but non-zero. Such a feature is not related to the VOF–PLIC algorithm, but to the number of iterations set for the augmented Lagrangian algorithm, so that much better results could be achieved at the expense of higher computation times. Unsurprisingly, the change in bubble volume is greater in the compressible framework, but the difference is globally small. As a conclusion the incompressibility hypothesis is relevant as long as the bubble rising path remains short. With larger distances, changes in static pressure are no longer negligible, and the compressible framework is a more relevant approach.

4.2. Example application: dynamics of compressible gas bubbles injected in liquid alloys

The example application presented in this section involves all physical issues for which the SVOF method has been designed: strong gradients on liquid-gas interface, multiple interface breakup and coalescence with surface tension effects, gas compressibility effects, and unusually high density and viscosity ratios across the interface. The target application relies on controlling the flow of liquid metals using gas injection techniques. The underlying challenge is first to predict bubbling to jetting transitions, then to use these results to achieve a better control of jet penetration. In its

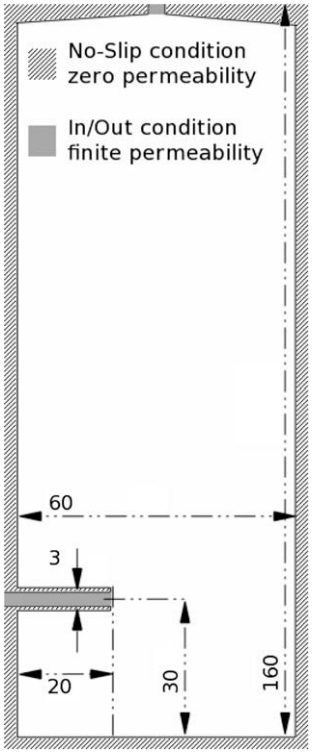

Fig. 9. Definition sketch for two-dimensional simulation of gas injection into cold liquid alloy. All dimensions are in millimeters.

Table 3
Simulation error levels based on terminal bubble rising velocity U_{Exp} as measured by Bhaga and Weber (1981). Target bubble shape as a function of Bond and Reynolds numbers (see Fig. 1), target bubble velocity. Error levels achieved with incompressible front-tracking method (Hua and Lou, 2007) on 300×100 grids ($d/\Delta x = 13$). Error levels and relative change in gas volume for incompressible and compressible SVOF methods on 600×200 grids ($d/\Delta x = 25$).

Test-Case	A1	A2	A3	A4	A5	A6	A7	A8
Shape	S	OE	OED	OEC	SCC	SCO	SKS	SKW
Bo	8.67	17.7	32.2	243	115	237	339	641
Re	0.98	1.67	79.9	15.24	134.6	357.0	30.83	49.72
U_{Exp} (m s^{-1})	0.0353	0.0615	0.307	0.226	0.309	0.321	0.263	0.270
εFront-tracking (%)	9.63	9.25	4.23	8.07	5.64	Unstable	2.12	1.22
εSVOF/incomp (%)	0.8	2.6	1.1	5.3	10.2	–	5.5	7.5
εSVOF/comp(%)	0.8	2.9	0.6	5.0	10.1	–	0.9	2.8
Δ*Volume*/incomp (%)	0.14	0.17	1.85	1.10	3.65	–	1.45	1.76
Δ*Volume*/comp (%)	0.25	0.28	1.95	1.18	3.77	–	1.51	1.81

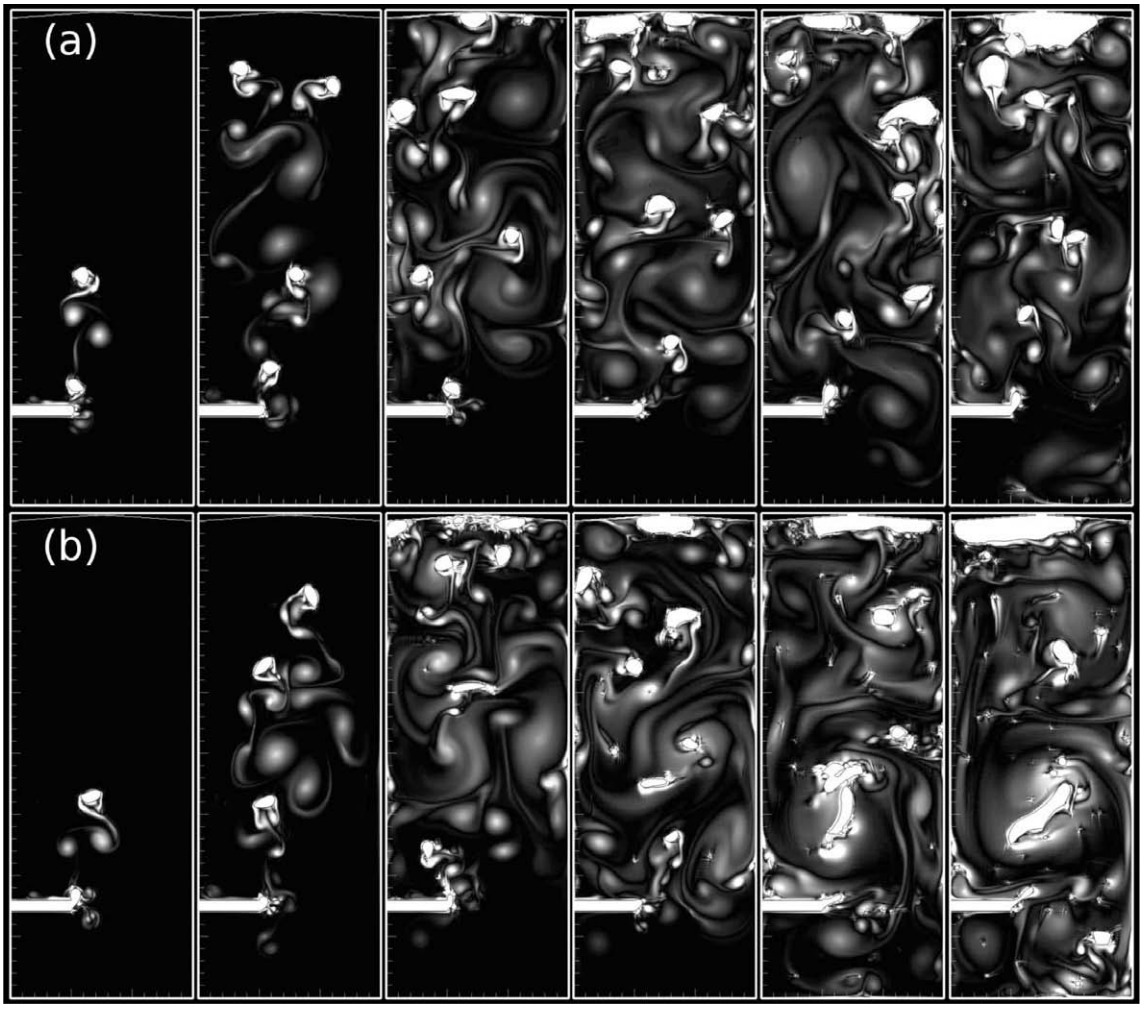

Fig. 10. Injection of gas bubbles into liquid metal. $\rho_{gas} = 2[\text{ kg m}^{-3}], \rho_{liquid} = 6360[\text{ kg m}^{-3}], \mu_{gas} = 2,26 \times 10^{-5}[\text{Pa s}], \mu_{liquid} = 1.89 \times 10^{-3}[\text{Pa s}]$. Compressible gas phase (a), incompressible gas phase (b). Snapshots of two-phase flow at times 0.5 s, 1 s, 2 s, 3 s, 4 s and 5 s. Gas phase (white level), contours of vorticity magnitude (grey levels).

present state, our work has focused on subjecting the simulation method to the same physical constraints as those observed experimentally (work still in process) but in two-dimensions, as a fundamental step prior to large-scale three-dimensional simulations that are planned in a near future. To this end, a virtual gas injection testing device has been designed (see Fig. 9). The testing configuration was set as a 16 cm high $\times$ 6 cm wide vessel. Gas is injected laterally through a horizontal pipe of internal diameter 3 mm which ends 3 cm away from the vessel's bottom and 2 cm away from the left wall. In order to achieve stable simulations in the case of incompressible gas injection, the vessel's top wall has been given a specific shape so as to collect rising bubbles and evacuate them through a 3 mm orifice. Physical characteristics are defined so that the liquid-to-gas density ratio is about 3500 and the liquid-to-gas viscosity ratio 84. As mentioned in Fig. 9, a porous medium model of finite permeability $K = 1 \times 10^{-15}$ m^2 is used in the injection pipe and in the evacuation tip as well, because it prevents the liquid metal, much heavier than gas, from drawing back into the capillary pipe since this always results in numerical failure. To our knowledge, this technique is of common use in various engineering applications for ensuring a steady gas flux (Nakai et al., 1985; Cahill, 2005). The input boundary condition is adjusted so as to recover injection velocity from one three-dimensional system of similar size in which gas flow-rate is 10 cm^3/min and pipe diameter is 3 mm. The Cartesian simulation grid size is 300 $\times$ 800, so that $\Delta x = 0.2$ mm. All simulations presented in this paper have been performed with a MPI parallelized code executed on eight processors, using a Linux cluster of quad-core 3 GHz Intel Xeon bi-processors. Simulations for both compressible and incompressible gas injection are performed and compared on Fig. 10. The gas phase is colored in white, grey levels represent magnitude of fluid vorticity. Two corresponding animations are proposed as supplemental multimedia files[1].

The release frequency is about five bubbles per second and there is no major differences of bubble size or velocity between the incompressible and compressible approaches, at least during the early stage of simulations. For information purposes, preliminary experimental observations for an equivalent bubble release frequency estimates the mean two-phase flow vertical velocity at $\simeq 0.1$ m s^{-1} in the bubble plume. In our simulations, the peak Reynolds number based on bubble size is $R_e = 4000$. The Bond number is $B_o \lesssim 8$ and the Weber number that can be used in three-dimensions to predict bubble fragmentation is $W_e = \rho_f U_t^2 d/\sigma \lesssim 2$. The upper R_e limit is roughly estimated using the maximum bubble velocity $U_b \simeq 0.15$ m s^{-1}. In practice our simulations predict that the mean two-phase flow regime is notably lower, say $Re \lesssim 2000$ since bubbles evolve in a non-quiescent velocity field. This is a transitional flow regime where energy is dissipated by large vortices, it is made clear in Fig. 10 where vorticity visualization reveals

[1] See Animation 1: 'incompressible gas injection into liquid metal', and Animation 2: 'compressible gas injection into liquid metal'.

large-scale structures generated in bubble wakes. Our results were calculated using direct numerical simulation but further work in the near future will necessarily involve Large Eddy Simulation (LES) techniques with specific turbulent two-phase LES terms presented in a recent work (Vincent et al., 2008).

From Fig. 10 one can note strong interactions between isolated pairs of bubbles, as the wake of a rising bubble induces a drifting effect on the following one, this is made clear particularly in the compressible case in which energy dissipation is more efficient and the bubble plume is consequently more stable. Energy dissipation confined in two-dimensions and subjected to wall containment have a major impact on bubble dynamics over long periods. Dissipation is much less efficient in the incompressible case, this is made clear in Fig. 10 as the bottom part of the domain exhibits important vorticity traces compared to the compressible case. Obviously, the excess of energy is contributing to a larger interface fragmentation, the distinction is in evidence after 4 s of simulation. Moreover, some of the smallest interface fragments are not advected by VOF and act as parasitic obstacles that degrade the global flow behavior. Those qualitative observations provide many indications to be considered in future three-dimensional simulations. It was made clear that considering gas compressibility reduces VOF numerical fragmentation and improves the simulation stability. Analogous simulations using VOF–PLIC with unprocessed surface tension and characteristic averaging are unable to converge due to excessive numerical fragmentation. Containment does have a major effect on bubble dynamics. Constrained fluid structures have a long lifetime due to the low viscosity of liquid metal. As a consequence, results show strong interactions between persistent fluid structures and bubbles, so that larger simulation domains are required to obtain a regular bubble plume with a steady injection and globally isotropic liquid drifting.

5. Concluding remarks

This work is the preliminary step of an ambitious project that is intended to predict and control gas injection into molten metals. This objective was partially fulfilled, as an original computational method has been designed and presented as one of the few operational simulation tools with the ability to handle two–phase flows with surface tension effects, compressibility effects, large density and viscosity contrasts. Benchmark verifications and comparison to popular interface tracking methods has proven the SVOF ability to preserve volume during interface advection in a much better way, affording a reasonable overcost. The predictions of the SVOF method has been successfully validated in two-dimensions against experimental and numerical methods for the dynamic of isolated gas bubbles evolving in an axisymmetric referential. Taking into account the effect of gas compressibility globally improved the accuracy of simulations. The method has been shown to be particularly stable when coping with strong interfacial distorsion and strong gradient of material properties met in gas/liquid metal multiphase systems. Work in the near future is intended to compare three-dimensional DNS/LES simulations and original X-ray radioscopic imaging of gas injected into cold liquid alloy.

Acknowledgements

The authors wish to thank the Aquitaine Regional Council for the financial support dedicated to a 256-processor cluster investment, located in the TREFLE laboratory. We are grateful for access to the computational facilities of the French CINES (National Computing Center for Higher Education), IDRIS (National Computing Center of CNRS) and CCRT (National Computing Center of CEA) under project number x2009026115.

Appendix A. Supplementary data

Supplementary data associated with this article can be found, in the online version, at doi:10.1016/j.ijmultiphaseflow.2009.12.002.

References

Amestoy, P.R., Duff, I.S., L'Excellent, J.-Y., 2000. Multifrontal parallel distributed symmetric and unsymmetric solvers. Comput. Methods Appl. Mech. Eng. 184, 501–520.
Bhaga, D., Weber, M.E., 1981. Bubbles in viscous liquids: shapes, wakes and velocities. J. Fluid Mech. 105, 61–85.
Bonometti, T., Magnaudet, J., 2007. An interface-capturing method for incompressible two-phase flows. Validation and application to bubble dynamics. Int. J. Multiphase Flow 33, 109–133.
Brackbill, J.U., Kothe, D.B., Zemach, C., 1992. A continuum method for modeling surface tension. J. Computat. Phys. 100, 335–354.
Cahill, V., 2005. Considering refractories. Foundry Manage. Technol. 100, 335–354.
Caltagirone, J.-P., Vincent, S., 2001. Sur une méthode de pénalisation tensorielle pour la résolution des équations de Navier–Stokes. Comptes Rendus de l'Académie des Sci. – Series IIB – Mech. 329, 607–613.
Caruyer, C, Vincent, S., Meillot, E., Caltagirone, J.-P., 2009. A two-phase LES compressible model for plasma-liquid jet interaction. In: 2nd International Conference on Turbulence and Interaction, 31st May–5th June, 2009 – Sainte-Luce, Martinique.
Delhaye, J.M., 1974. Jump conditions and entropy sources in two-phase systems. Local instant formulation. Int. J. Multiphase Flow 1, 395–409.
Esmaeeli, A., Tryggvason, G., 1998. Direct numerical simulations of bubbly flows. J. Fluid Mech. 377, 313–345.
Fortin, M., Glowinski, R., 1982. Méthodes de lagrangien augmenté. Application à la résolution numérique de problèmes aux limites. Dunod.
Glowinski, R., Pan, T.-W., Hesla, T.I., Joseph, D.D., Périaux, J., 2001. A fictitious domain approach to the direct numerical simulation of incompressible viscous flow past moving rigid bodies: application to particulate flow. J. Computat. Phys. 169, 363–4260.
Gopala, V.R., van Wachem, B.G.M., 2008. Volume of fluid methods for immiscible-fluid and free-surface flows. Chem. Eng. J. 141, 204–221.
Harlow, F.H., Welch, J.E., 1965. Numerical calculation of time-dependent viscous incompressible flow of fluid with free surface. Phys. Fluids 8, 2182–2189.
Hua, J., Lou, J., 2007. Numerical simulation of bubble rising in viscous liquid. J. Computat. Phys. 222, 769–795.
Hysing, S., Turek, S., Kuzmin, D., Parolini, N., Burman, E., Ganesan, S., Tobiska, L., 1999. Quantitative benchmark computations of two-dimensional bubble dynamics. Int. J. Numer. Methods Fluids 60, 1259–1288.
Inamuro, T., Ogata, T., Tajima, S., Konishi, N., 2004. A lattice boltzmann method for incompressible two-phase flows with large density differences. J. Computat. Phys. 198, 628–644.
Jamet, D., Lebaigue, O., Coutris, N., Delhaye, J.M., 2001. The second gradient theory: a tool for the direct numerical simulation of liquid–vapor flows with phase-change. Nucl. Eng. Des. 204, 155–166.
Jiang, G.-S., Shu, C.-W., 1996. Efficient implementation of weighted eno schemes. J. Computat. Phys. 126, 202–228.
Kataoka, I., 1986. Local instant formulation of two-phase flow. Int. J. Multiphase Flow 12, 745–758.
Khadra, K., Angot, P., Parneix, S., Caltagirone, J.-P., 2000. Fictitious domain approach for numerical modelling of Navier–Stokes equations. Int. J. Numer. Methods Fluids 34, 651–684.
Nakai, H., Murakami, M., Ichikawa, N., 1985. Flow of He 2 through porous-plug phase separators. In: Proceedings of the Symposium on Mechanics for Space Flight, (SEE N86-23858 14-34):135–156. and Caltagirone.
Osher, S., Fedkiw, R., 2003. Level set methods and dynamic implicit surfaces. Appl. Math. Sci. 153, 1–10.
Peskin, C.S., 1977. Numerical analysis of blood flow in the heart. J. Computat. Phys. 25, 220.
Ritz, J.B., Caltagirone, J.-P., 1999. A numerical continuous model for the hydrodynamics of fluid particle systems. Int. J. Numer. Methods Fluids 30, 1067–1090.
Roache, Patrick J., 1998. Verification and Validation in Computational Science and Engineering. Hermosa Publishers.
Scardovelli, R., Zaleski, S., 1999. Direct numerical simulation of free-surface and interfacial flow. Annu. Rev. Fluid Mech. 31, 567–603.
Shin, S., Juric, D., 2002. Modeling three-dimensional multiphase flow using a level contour reconstruction method for front tracking without connectivity. J. Computat. Phys. 180, 427–470.
Tanguy, S., Berlemont, A., 2005. Application of a level set method for simulation of droplet collisions. Int. J. Multiphase Flow 31, 1015–1035.
Trontin, P., Vincent, S., Estivalezes, J.-L., Caltagirone, J.-P., 2008. Detailed comparisons of front-capturing methods for turbulent two-phase flow simulations. Int. J. Numer. Methods Fluids 56, 1543–1549.
Tryggvason, G., Bunner, B., Esmaeeli, A., Juric, D., Al-Rawahi, N., Tauber, W., Han, J., Nas, S., Jan, Y.-J., 2001. A front-tracking method for the computations of multiphase flow. J. Computat. Phys. 169, 708–759.
Unverdi, S.O., Tryggvason, G., 1992. A front-tracking method for viscous, incompressible, multi-fluid flows. J. Computat. Phys. 100, 25–37.

Vincent, S., Caltagirone, J.-P., 1999. Efficient solving method for unsteady incompressible interfacial flow problems. Int. J. Numer. Methods Fluids 30, 795–811.

Vincent, S., Caltagirone, J.-P., 2000. A one-cell local multigrid method for solving unsteady incompressible multiphase flows. J. Computat. Phys. 163, 172–215.

Vincent, S., Caltagirone, J.-P., Lubin, P., Randrianarivelo, T.N., 2004. An adaptative augmented lagrangian method for three-dimensional multimaterial flows. Comput. Fluids 33, 1273–1289.

Vincent, S., Randrianarivelo, T.N., Pianet, G., Caltagirone, J.-P., 2007. Local penalty methods for flows interacting with moving solids at high reynolds numbers. Comput. Fluids 36, 902–913.

Vincent, S., Larocque, J., Lacanette, D., Toutant, A., Lubin, P., Sagaut, P., 2008. Numerical simulation of phase separation and a priori two-phase les filtering. Comput. Fluids 37, 898–906.

Youngs, D.L., Morton, K.W., Baines, M.J., 1982. Time-dependent multimaterial flow with large fluid distortion. Numerical Methods for Fluid Dynamics. Academic Press, New York.

Yue, P., Feng, J.J., Bertelo, C.A., Hu, H.H., 2007. An arbitrary lagrangian–eulerian method for simulating bubble growth in polymer foaming. J. Computat. Phys. 226, 2229–2249.